Dielectric relaxation and electrical conductivity property correlation in Gd-doped BBTO Aurivillius ceramics

K. S. K. R. Chandra Sekhar[1] · Tirupathi Patri[2] · Ammar Mohamed Tighezza[3] · Deepash Shekhar Saini[4] · P. Rosaiah[5] · Avijit Ghosh[6]

Abstract

Gd ion-substituted barium bismuth titanate ($BaBi_4Ti_4O_{15}$; BBTO) Aurivillius ceramics were synthesized to understand the preliminary impact through the structural, optical, frequency-dependent dielectric, conductivity, and complex modulus spectroscopic studies. X-ray diffraction (XRD) study confirmed the phase purity and crystallinity of the orthorhombic crystal system with $A2_1am$ space group. The room temperature *Raman study* was correlated with the XRD results revealing a more feasible Aurivillius phase. A shift in the Curie temperature (T_m) towards low-temperature regions with increasing concentrations of Gd dopant was observed in temperature-dependent conductivity studies. The frequency-dependent conductivity study revealed a diffuse relaxor signature that degraded with dopant concentration explained by the modified Curie–Weiss law and normalized dielectric permittivity study. The frequency and temperature dependent modulus spectroscopic study indicated a dielectric relaxation mechanism in the presence of doubly ionized oxygen vacancies in pristine BBTO ceramics whereas the dominance of singly ionized oxygen vacancies was observed in Gd-doped one. The dielectric relaxation mechanism for pristine and doped Aurivillius are explained due to the thermal motion of the localized hopping process of electrons in variable oxidation states of different single ionized ions that depart from ideal Debye behavior. A detailed ac-conductivity study revealed the jumping relaxation mechanism or correlated barrier hopping mechanism (CBM) because of the localization of charge carriers, or the formation of polarons, respectively.

✉ Tirupathi Patri
  ptirupathi36@gmail.com

✉ Avijit Ghosh
  avijitphy@gmail.com

[1] Department of Physics, V. R. Siddhartha Engineering College, Vijayawada, Andhra Pradesh 520007, India

[2] Department of Physics, Rajiv Gandhi University of Knowledge Technologies, Srikakulam, Andhra Pradesh 532402, India

[3] Department of Chemistry, College of Science, King Saud University, P. O. Box 2455, 11451 Riyadh, Saudi Arabia

[4] Department of Physics, Deen Dayal Upadhaya Gorakhpur University, Gorakhpur, Utter Pradesh 273009, India

[5] School of Mechanical Engineering, Yeungnam University, 280 Daehak-Ro, Gyeongsan-Si, Gyeongsangbuk-Do 38541, Republic of Korea

[6] Departments of Physics, Central University of Jharkhand, Ranchi, Jharkhand 835205, India

Graphical abstract
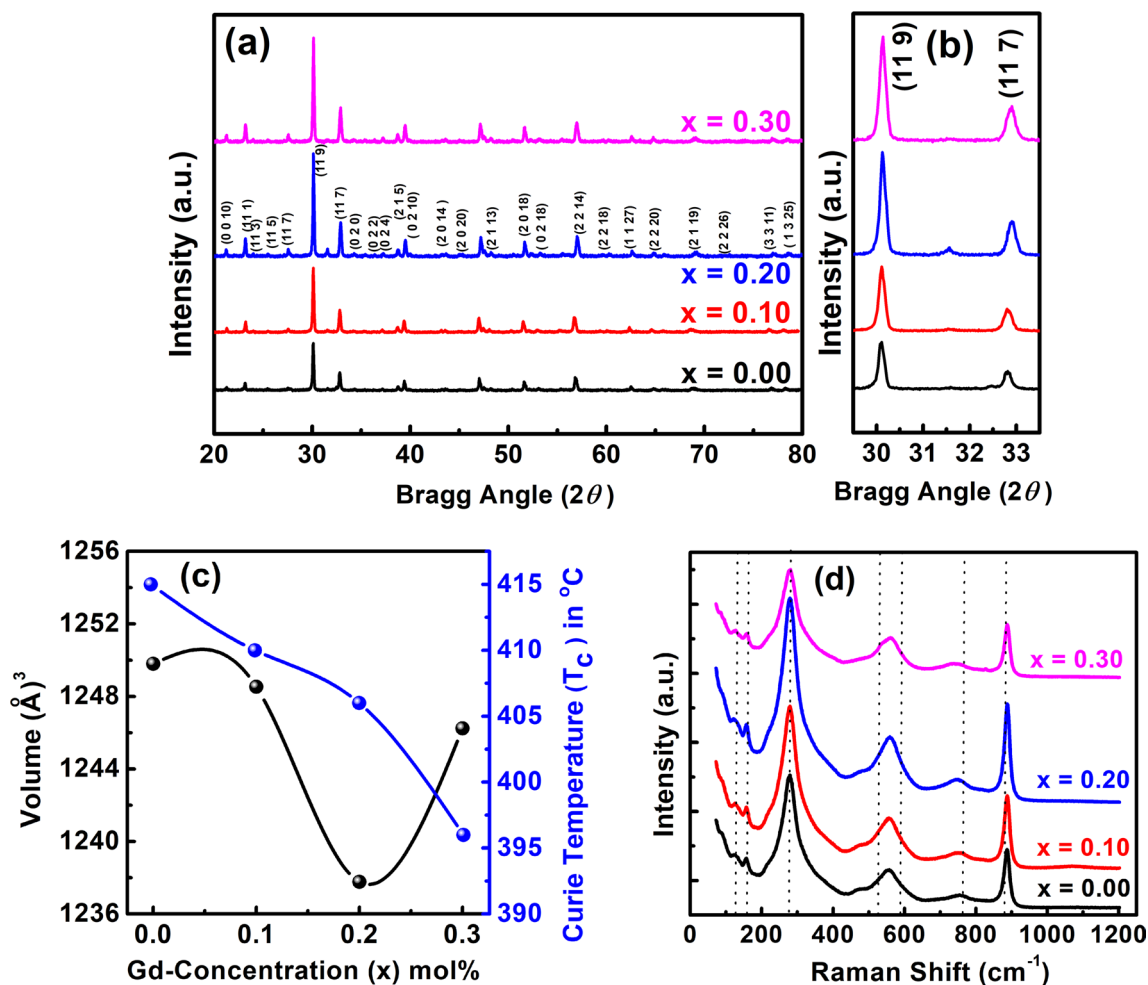
Keywords Aurivillius ceramics · Orthorhombic crystal system · Complex impedance · Conductivity · Dielectric relaxation

1 Introduction

Ferroelectric, relaxor, and anti-ferroic materials are considered promising candidates for next-generation practical electronic device applications such as energy storage devices, transducers, and sensors owing to their large dielectric permittivity and significant polarization induced by the applied field [1–3]. A few decades ago, a new group of Bismuth-based layered structure ferroelectric materials was discovered by Aurivillius, termed as "Aurivillius compounds" or Bismuth Layer-Structured Ferroelectrics. In general, Aurivillius layered ferroelectrics have attracted much attention because of their large spontaneous polarization (P_s) tunable with external fields, high Curie temperatures (T_c), desirable relaxor ferroelectric behavior, and good resistance to polarization fatigue [4, 5]. Aurivillius materials are generally formulated as $(A_{n-1}B_nO_{3n+1})^{2-}$ $(Bi_2O_2)^{2+}$, where n denotes

the layer or number of pseudo-perovskites inserted between the $(Bi_2O_2)^{2+}$ layers. The general structure of Aurivillius is a $(A_{n-1}B_nO_{3n+1})^{2-}$ pseudo-perovskite unit cell sandwiched between two fluorite-like $(Bi_2O_2)^{2+}$ layers along the c-axis. In the general formula, A represents monovalent, divalent, or trivalent cations with a 12-fold coordinated interstice, while B represents tetravalent, pentavalent, or hexavalent cations, either individually or in combination, with a nine-fold coordinated site. The variable 'n' is an integer, often between 1 and 5, which represents the number of BO_6 octahedral [5, 6].

Among the reports within Aurivillius group, more attention is drawn to $n = 3$ and $n = 4$ layers i.e., the bismuth compounds $Bi_4Ti_3O_{12}$ ($n = 3$) and $Bi_5Ti_4O_{15}$ ($n = 4$). These two series of materials are highly tunable due to various ionic substituents and are recognized for their advanced multifunctional characteristics including optical, piezoelectric, and relaxor ferroelectric properties [2, 5, 7]. The classical

ferroelectricity originates from the $n = 4$ ($Bi_5Ti_4O_{15}$) layered compounds of Aurivillius materials through the substitution of di-valent elements at the Bi-site, which is denoted as $ABi_4Ti_4O_{15}$ (ABTO) series (where A = Ba, Sr, Ca). Within the ABTO series, the ceramics $BaBi_4Ti_4O_{15}$ (BBTO) have gained more attention owing to their relaxor ferroelectricity, large spontaneous polarization, and anti-fatigue properties. These ceramics also exhibit additional strong bond internal structural connections, involving $(Bi_2O_2)^{2+}$ and $(BaBi_2Ti_4O_{13})^{2-}$ units, in contrast to the typical Aurivillius ceramics of $SrBi_4Ti_4O_{15}$ and $CaBi_4Ti_4O_{15}$ [8–11]. In addition, the $BaBi_4Ti_4O_{15}$ (BBTO) ceramics exhibit an appreciable piezoelectric coefficient, making them suitable for electro strictive applications. Coupled with their relaxor ferroelectric nature, optimistic for these ceramics hold promise for potential electro-caloric applications. Although BBTO are known for their potential in practical applications, the high sintering temperature of BBTO can be disadvantageous due to the liberation of oxygen vacancies caused by the volatile nature of bismuth ions. These oxygen vacancies trigger a charge imbalance, thereby reducing the electrical resistivity and consequently leading to a high occurrence of leakage current in BBTO Aurivillius compounds. In addition, at very high-temperatures, low dielectric loss with high fatigue ferroelectricity leads to astonishing real applications [8, 12, 13]. To overcome these drawbacks, researchers are motivated to investigate dielectric and electrical characterizations of divalent, trivalent, and rare earth (RE) element substituted BBTO Aurivillius ceramics.

Among the dopant elements, rare earth elements are more favorable for the ferroelectric distortion of bismuth-containing compounds because of weakening of the Bi–O hybridization and induction of ionic size effect. The doping of rare earth ions can reduce the defect induced dielectric behavior, suppressing leakage current while simultaneously improving the electrical properties of Bi-based materials [14, 15]. The dielectric behavior and conduction mechanism of grain interiors and grain boundaries play a central role in the dielectric relaxation and electrical properties of Bi-based ceramics. To investigate the effect of defect behaviors in ceramics, distinguish the electrical contributions of grains, grain boundaries and electrode interfaces, and study the phase transitions temperature dependent dielectric and conductivity, is required. Literature reports on RE doped BBTO ceramics are confined, with Sm, Nd and La doped BBTO ceramics being the most frequently identified [14–18]. Based on these motives, the detailed structural and microstructural correlations were investigated in relation to dielectric and electrical property analyses. A brief overview, the contribution of both grain interiors and grain boundaries to the electrical properties was investigated through conductivity and electrical modulus analyses. Dielectric relaxation processes and conduction mechanisms are discussed in the context of kinetic analysis.

2 Experimental details

Aurivillius Gd-doped $BaBi_{4-x}Gd_xTi_4O_{15}$ 4-layered oxides ($x = 0.00$, 0.10, 0.20 and 0.30) ceramics were synthesized by conventional solid-state reaction using high-purity of Bi_2O_3 (99.99% purity), TiO_2 (99% purity), $BaCO_3$ (99% purity), and Gd_2O_3 (99.9%) powders. All the ingredients are taken in stoichiometric amounts and thoroughly using an agate mortar and pestle in presence of acetone medium to obtain a homogeneous mixture. Due to evaporation of Bismuth oxide, an additional 5 wt% Bi_2O_3 was added to the mixture to compensate for its loss in the final compound. Multiple calcinations were carried out at 850 °C and 900 °C for 4 h after repeated grinding using acetone as the medium [19, 20]. The phase purity and crystallinity were examined using an X-ray diffractometer (PHILIPS-PW3373 XPERT-PRO) within the angular range $10º \leq 2\theta \leq 80º$. Furthermore, to study the physical properties such as dielectric characterization, pellet making process was carried out using 5% polyvinyl alcohol (PVA) as a binder. Following pellets formation, sintering was carried out at 1100 °C in 4 h to obtain dense pellets. The sintered pellets were coated with silver (Ag) electrodes on its compact surfaces and dried at 200 °C for 12 h. Then, the temperature dependent dielectric measurements were carried out with Wayne Kerr 6500B impedance analyzer in a temperature range from 30 to 500 °C and frequencies ranging from 100 Hz to 1 MHz. The identification of internal spin-phonon mode of the Aurivillius ceramics was carried out using a micro-Raman spectrometer (Witac Alpha 300) with a 532 nm excitation source in the wavenumber range from 50 to 1000 cm^{-1} [21].

3 Results and discussion

3.1 Structure and microstructural studies

Figure 1a illustrates the room temperature X-ray diffraction (XRD) pattern of Gd-substituted $BaBi_{4-x}Gd_xTi_4O_{15}$ ($x = 0.00$, 0.10, 0.20, and 0.30) 4-layered Aurivillius ceramics. Preliminary XRD study confirms the crystallinity and phase purity of the Aurivillius ceramics. The observed pattern was [9] indexed (ICSD-99501: $n = 4$) with a non-centrosymmetric orthorhombic crystal system for the $A2_1am$ space group, which also matches recent reports [8, 9, 14]. This is verified for all Gd doped BBTO phases and is consistent with previous reports [10, 11]. A drastic change in intensity was observed with index planes (119) and (117) as Gd^{3+} dopant concentration increased, indicating substitution of Gd at Bi-site either layered
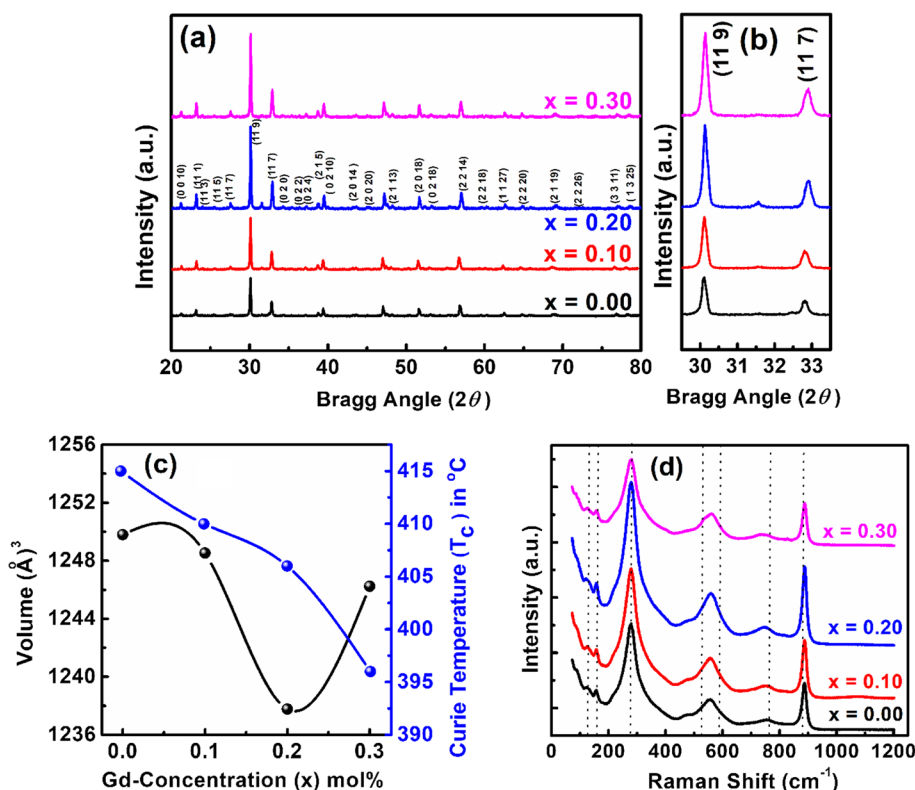
[Bi$_2$O$_2$]$^{2-}$ or tetrahedral site of (BaBi)TiO$_3$ component. This resulted in a decrease in tensile stress, leading to a reduction in the volume of the unit cells. This change played a key role in the variation of maximum index profile peak intensity. Furthermore, a clear decrease in unit cell volume due to Gd substitution was noticed in Fig. 1c. To determine the influence of Gd substitution on the structure of BBTO ceramics, Rietveld refinement was carried out using the Fullprof software. The refinement was fitted to the orthorhombic crystal system with A2$_1$am space group, which also agreed with the previous report [19]. The detailed refinement process and consequence of the structural changes were explained, where required Rietveld refinement plots as shown as Supplementary Fig. 1.

To determine the vibrational modes of atoms within both pristine and Gd-substituted BBTO ceramics, Raman spectroscopic measurement was carried out. The wavenumber modes altered by the phonon correlation of atoms, such as vibrational modes due to internal stacking of [Bi$_2$O$_2$]$^{2+}$ layers along with perovskite unit cell [BaBi$_2$Ti$_4$O$_{13}$]$^{2-}$ atoms, can be visualized with help of Raman spectroscopic technique. The room temperature Raman spectrum of pristine and Gd-doped BBTO ceramics is shown in Fig. 1d. The collected Raman spectrum ranges from 55 to 1000 cm^{-1} and includes a few known modes at 64, 127, 157, 278, 486, 555, 753, and 887 cm^{-1} which were observed [17, 22]. The internal structure of

BBTO Aurivillius layered perovskite ceramics is associated with two regular stacking of fluorite-like [Bi$_2$O$_2$]$^{2+}$ slabs and perovskite-like [BaBi$_2$Ti$_4$O$_{13}$]$^{2-}$ blocks. The first one has an internal Bi^{3+} ion contained within two sites: one at the [Bi$_2$O$_2$]$^{2+}$ layers where Bi$_2$ have coordination number (CN) of 8, and the other at the A-site for [BaBi$_2$Ti$_4$O$_{13}$]$^{2-}$ blocks where BaBi$_2$ adopts CN of 12. In association with the above, the Raman spectra are categorized into three parts based on wave number region, i.e., low frequency modes below 200 cm^{-1}, medium modes from 200 to 800 cm^{-1}, and higher modes above 800 cm^{-1}. The low frequency modes are related to (Bi$_2$O$_2$)$^{2+}$ layers of the perovskite unit cell [BaBi$_2$Ti$_4$O$_{13}$]$^{2-}$. The vibrational modes for the A-site of the pseudo-perovskite layer are identified at 64, 127 and 157 cm^{-1}. The first one at 64 cm^{-1} is independent of Gd-substitution, and the other two modes at 127 and 157 cm^{-1} indicate a decrease in intensity, that signs a proper substitution of foreign ions in A-site. Furthermore, the medium range frequencies modes appear at 278, 486, 555, 753 cm^{-1}, corresponding to torsional and bending vibration of TiO$_6$ octahedra and Ba–O bond [19, 20, 23]. The upper frequency mode observed at 887 cm^{-1} is attributed to the stretching mode of TiO$_6$ octahedra and the BiO$_6$ octahedral stretching vibration in BBTO ceramics [22]. Therefore, these results are more suitable to support the XRD pattern, which is a direct representation of the substitution of Gd^{3+} ion at Bi-site

Fig. 2 Depiction of crystallographic unit for Gd substituted ceramic $x = 0.10$
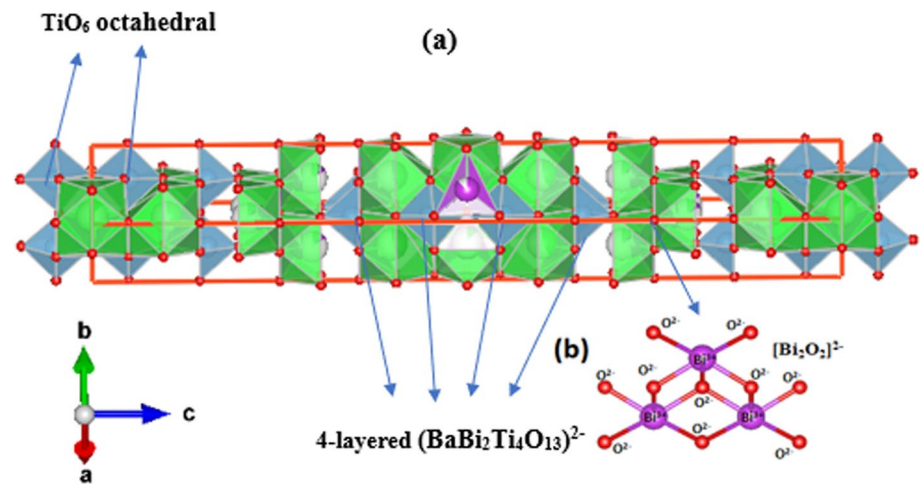
in BBTO Aurivillius ceramics. Additionally, the crystallographic unit cell for the Gd – substituted BBTO ceramic $x = 0.10$ has been depicted in Fig. 2.

4 Temperature dependent dielectric study

The dielectric permittivity and loss tangent are two important parameters to investigate the temperature dependent phase transitions, as reported elsewhere in the present prepared samples [19, 20]. For more clarity, temperature dependent dielectric permittivity at a fixed frequency (100 kHz) for all Gd-doped BBTO ceramics is illustrated in Fig. 3a. A brief discussion of relaxor activity with frequency dependency has been presented in previous reports [24]. In support with the previous findings, it is mentioned that diffuse relaxor activity predominates in the pristine BBTO compound during the paraelectric to ferroelectric transition at 415 °C. This is known as the Curie temperature (T_m), as shown in Fig. 3a. A decrease in the Curie temperature (T_m) is observed with Gd-doped BBTO ($x = 0.10$, 0.20, and 0.30), as shown Fig. 3a.

These observed experimental results are consistent with the previous literature [11, 20, 23, 24]. The substitution of Gd^{3+} ion in BBTO compound at the A-site $(Bi_2O_2)^{2+}$ layers or perovskite unit cell $[BaBi_2Ti_4O_{13}]^{2-}$ ($BaBi_2$ site) is affected because of a decrease in internal stacking bond angles. Therefore, a decrease in unit cell volume was observed due to discrepancy in the ionic radii of Bi^{3+} (1.17 Å) and Gd^{3+} (0.94 Å) ions. Consequently, the decrease in orthorhombicity leads to a decrease in Curie temperature (T_m) in Gd^{3+} doped BBTO ceramics as noticed. Furthermore, it is noticed that a decrease in grain size and increase in thickness of plate like grains, as detected in surface morphology studies were also reported elsewhere [24, 25]. Thus, it is also main reason for decrease in orthorhombicity, hence a decrease in T_m towards the low temperature regime.

The phase transition can be explained by examining the dielectric permittivity peak profile as a function of temperature. The dielectric permittivity peak's diffuseness at T_m establishes a correlation to the relaxor ferroelectric character. The diffuseness of the maximum value of dielectric permittivity with respect to the applied field frequency near T_m

Fig. 3 **a** The variation of dielectric permittivity with temperature at a frequency of 100 kHz, and **(b)** The modified Curie–Weiss law fitting plot (Inset: A plot of normalized dielectric permittivity with temperature) for the Gd-substituted $BaBi_{4-x}Gd_xTi_4O_{15}$ ceramics from $x = 0.00$ to 0.30, respectively
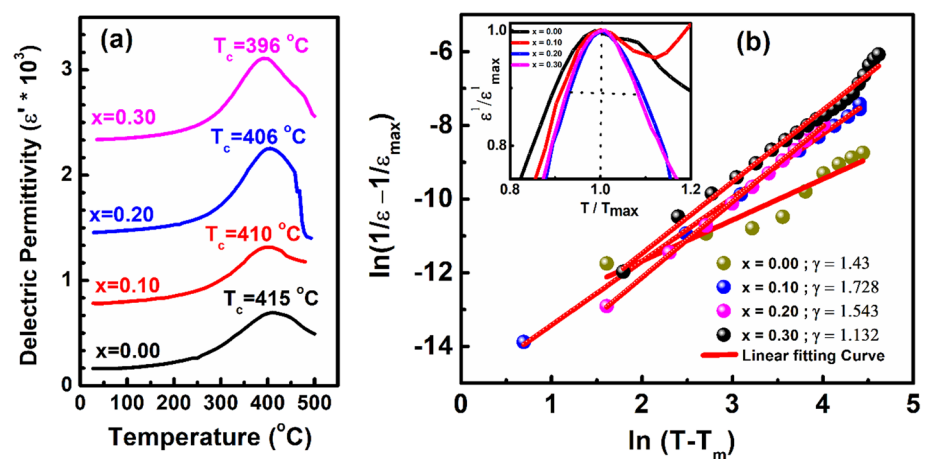
can be fitted using the modified Curie–Weiss law or Power law proposed by Uchino and Nomura, as shown in Eq. 1 [21, 25, 26].

$$\frac{1}{\varepsilon'} - \frac{1}{\varepsilon'_{max}} = \frac{(T - T_m)^\gamma}{C} (T > T_m) \tag{1}$$

where ε'_{max} is the maximum dielectric constant at T_m, C is the Curie constant, T is the absolute temperature and γ is the degree of diffuseness or diffusivity ($1 \leq \gamma \leq 2$). The diffusivity $\gamma = 1$ is for normal ferroelectrics, and $\gamma = 2$ for relaxor ferroelectrics [27]. Here, the diffuse relaxor activity can be systematically elucidated by fitting the dielectric plot ln $(\frac{1}{\varepsilon'} - \frac{1}{\varepsilon'_{max}})$ vs. ln (T–T_m) at a 1 MHz frequency, as shown in Fig. 3b [27]. The obtained γ values are 1.43, 1.73, 1.513, and 1.145 for $x = 0.00$, 0.10, 0.20, and 0.30, respectively. The initial value for the pristine compound is low, but it reaches maximum at $x = 0.10$ concentration. After that, it starts to decrease with substituent, indicating that the diffusivity decreases with the dopant. The observed diffuse relaxor signature is attributed to random redistribution of several cations at the A-site (i.e., Gd^{3+}, Bi^{3+} and Ba^{2+} ions) in $(Bi_2O_2)^{2+}$ layers or the perovskite $[BaBi_2Ti_4O_{13}]^{2-} BaBi_2$ sites. The local inhomogeneous distribution of barium and Gd^{3+} ions into $(Bi_2O_2)^{2+}$ layers, along with charge imbalances due to anti-site defects at A-site ions, easily leads to a structural distortion. This clearly emphasizes the greater diffuse activity in Gd^{3+} ion doped BBTO ceramics with certain limited composition substituents. Furthermore, the strength of diffusivity explained with help of normalized dielectric constant vs. normalized temperature graphs ($\frac{\varepsilon'_r}{\varepsilon_{max}}$ vs. $\frac{T}{T_{max}}$), as shown in inset of Fig. 3b [26]. The width of the normalized graphs remains unchanged up to $x = 0.10$, and then decreases for $x > 0.10$ concentrations. Hence, it can be concluded that the higher substituent levels at $x > 0.10$ stabilize the material towards classic ferroelectric character.

5 Temperature dependent modulus spectroscopy

To reveal the relationships between the diffuse dielectric relaxation mechanism and relaxor permittivity processes, both in frequency and temperature domains, the spectra of the Gd-doped BBTO compounds must discuss by adopting modulus spectroscopy. The modulus spectra, employed to analyze the inverse of dielectric permittivity, can be expressed as given in Eq. 2.

$$M^* = M' - \widehat{j}M'' = \frac{1}{\varepsilon^*}. \tag{2}$$

Figure 4a and b illustrates the temperature dependent real part of modulus spectra within fixed frequency regimes. As

Fig. 4 a–d The modulus spectroscopy curves with variation of temperature for the Gd-substituted $BaBi_{4-x}Gd_xTi_4O_{15}$ ceramics from $x = 0.00$ to 0.30, respectively
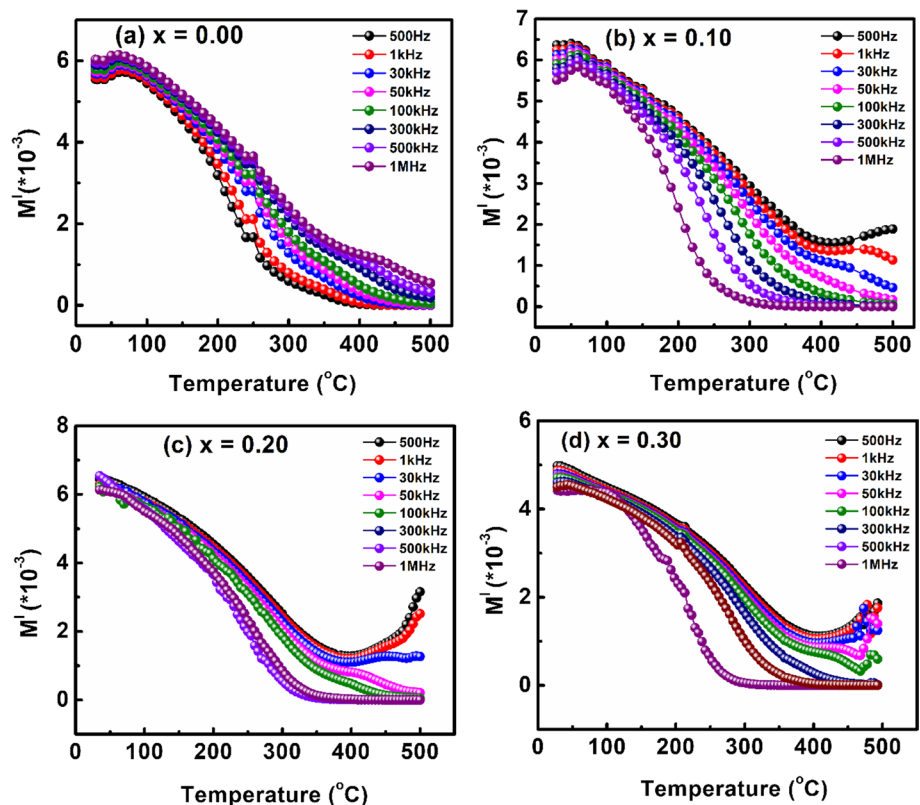
shown in Fig. 4, three distinct regions were noticed over a wide range of temperatures. In Region-I, from RT to 100 °C, a slight flatness in the modulus spectra was noticed. In the second distinct region-II, spanning from 150 to 350 °C, a significant decrement was observed. At high temperature, beyond 380 °C (> T_m), remarkable peaks were noticed for Gd-doped BBTO ceramics, attributed to the paraelectric–ferroelectric transition, which is consistent with our previous reports [28]. These peaks signify a relaxation mechanism associated with specific temperature intervals, further explored in the imaginary part of modulus spectroscopy studies. Figure 5a–d illustrate the imaginary part of modulus spectroscopy with temperature variation at fixed frequency intervals for all measured ceramics. There is no change in imaginary modulus value up to 100 °C; however, after that point, a monotonic increase in M'' was noticed several important points were investigated for all the measured samples: (i) A monotonous increase in M'' with the rise in temperature (with a single peak) in the measured temperature range for all observed frequencies, (ii) A clear appearance of a peak at a particular temperature (known as relaxation frequency, (f_0), (iii) A decrease in the magnitude of M'' with a clear shift in peak frequency towards the higher temperature side with the increased fixed frequency points, and (iv) Characteristic peak broadening with a rise in frequency. All these observations directly represent the occurrence of temperature dependent electrical phenomena in all Gd-doped materials. At very high temperature regions,

the spectra broadened at the high-frequency side, showing a departure from the ideal Debye behavior. To identify the presence of charge carriers within measured temperature intervals, the Arrhenius law (Eq. 3) was adopted to analyze different contributions of the electrical behavior in different regimes.

$$f = f_0 \exp^{-\left(\frac{E_a}{K_B T}\right)}. \tag{3}$$

Figure 6 depicts the variation of frequency with the temperature at fixed relaxation points {log (f) vs. 10^3/T}. According to the Arrhenius law, one can determine the
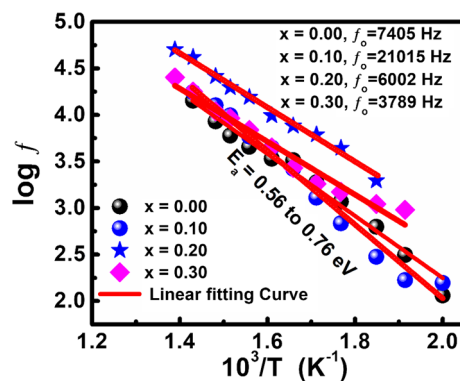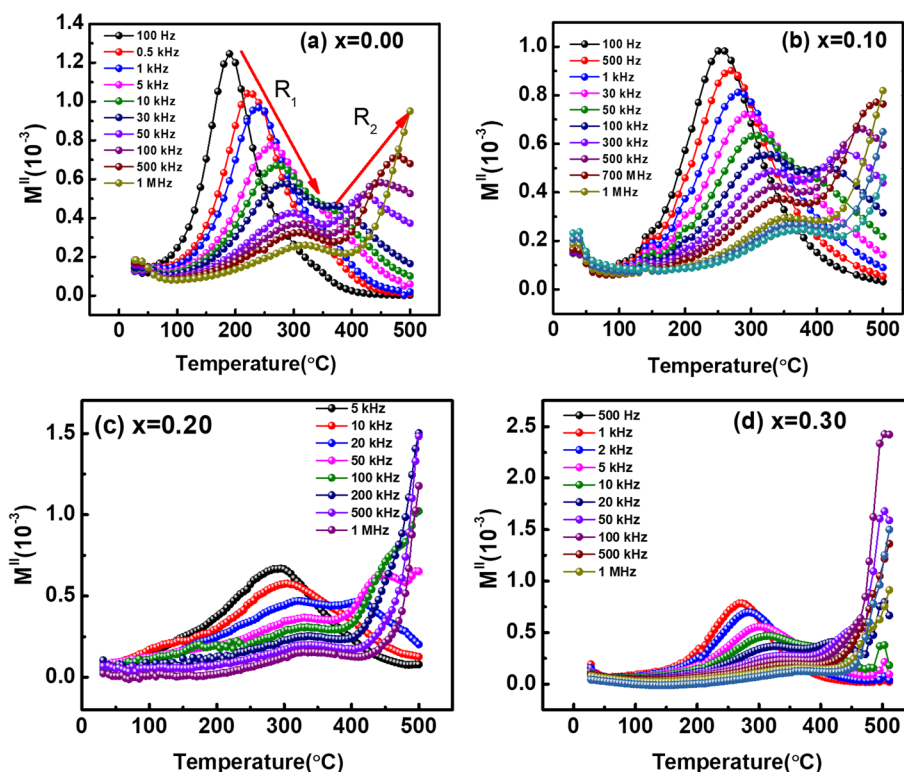
Fig. 6 The plots of log f vs. 10^3/T for Gd-substituted BaBi$_{4-x}$Gd$_x$Ti$_4$O$_{15}$ ceramics from $x = 0.00$ to 0.30

Fig. 5 **a–d** The imaginary part of modulus spectroscopy curves with the variation of temperature at fixed frequencies for the Gd-substituted BaBi$_{4-x}$Gd$_x$Ti$_4$O$_{15}$ ceramics from $x = 0.00$ to 0.30, respectively

activation energy by performing a linear fit of the temperature dependence of relaxation frequency (f), where f_0 is the maximum peak frequency, k_B is the Boltzmann constant, E_a is the activation energy for the mobility of free charges and T is the absolute temperature. The reciprocal of frequency is referred to as time period as expressed in terms of Arrhenius Eq. 4.

$$\tau = \tau_o \exp\left(\frac{-E_a}{k_B T}\right). \tag{4}$$

For undoped BBTO compound the observed activation energy is $E_a = 0.57$ eV, while for the Gd substituted BBTO compounds a single relaxation peak was observed. This peaks corresponds to an activation energy ranging from 0.45 to 0.75 eV, as presented in the inset of Fig. 6. These observations are consistent with the dominance of relaxation mechanism caused by the creation of singly ionized oxygen vacancies or defects resulting from the volatile nature of Bi-ions during high temperature sintering process [29–31]. A clear trend emerges as the amount of Gd-dopant in BBTO compounds increases, with a noticeable decrease in both the obtained activation energy and the free relaxation time. In Bi-based perovskite ceramics, during the high temperature sintering process, bismuth vacancies inevitably lead to the formation of oxygen vacancies in order to maintain the charge neutrality and balance of oxidation states. The conduction mechanism for electrons in perovskite structure oxides may be written as:

$$V_O \iff V_O^{'} + e^{'}, \tag{5}$$

$$V_O^{'} \iff V_O^{''} + e^{'}, \tag{6}$$

where $V_O^{'}$, $V_O^{''}$ are referred to as single and double ionized oxygen vacancies, respectively. In this case, the ionization of oxygen vacancies results in the creation of electrons. These electrons may form weakly bonds with B-site ions (Ti^{4+} ions). The overall reaction can be described using the following Kroger–Vink notation:

$$Bi_2O_3 \rightarrow 2Bi + \frac{3}{2}O_2 + 2V_{Bi}^{''} + 3V_O^{'}. \tag{7}$$
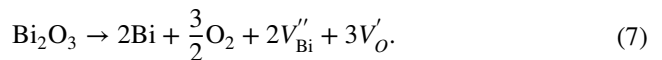
6 Frequency-dependent modulus spectroscopy

Considering the basic law for a small capacitance with large resistance, the induction of a hidden dielectric relaxation mechanism can be realized with the help of the frequency dependent modulus spectroscopic techniques in low frequency regions. Figure 7a–d illustrate the variation of M'

Fig. 7 **a**–**d** The real part of modulus spectroscopy with the variation of frequency at fixed temperatures for the Gd-substituted $BaBi_{4-x}Gd_xTi_4O_{15}$ ceramics from $x = 0.00$ to 0.30, respectively
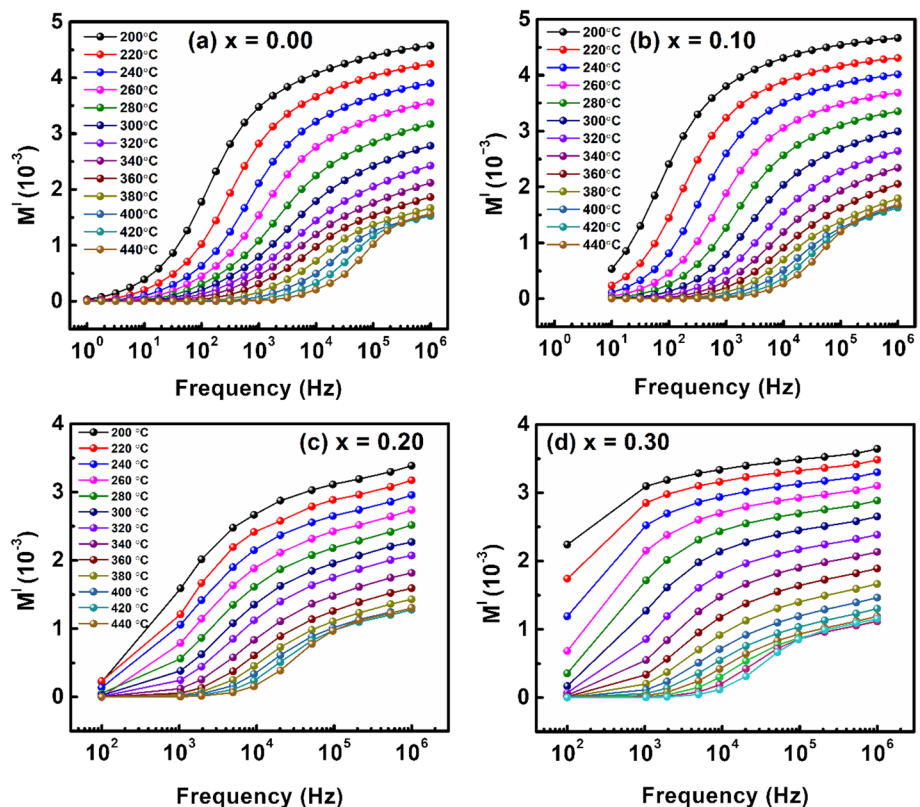
with frequency (f) at fixed temperature intervals ranging from 200 to 500 °C for all concentrations. It is noticed that a frequency dependent relaxation mechanism exists in a single region for the pristine compound. In the doped ceramics, a similar frequency dependent relaxation mechanism is observed, with a deep sleep-in frequency indicated as denoted in Fig. 7b–d with arrow indicators [32, 33]. To explore the presence of charge carriers responsible for the origin of relaxation phenomena, the variation of imaginary part of modulus with frequency graph with frequency graph in the temperature range from RT to 500 °C for all the samples is shown in Fig. 7a–d. It is found that the peaks of M'' are shifted towards higher frequency region with increase of temperature for all measured samples. This implies that the presence of typical single type of thermally activated charge carriers are more prominent. In the doped samples, M''-modulus spectra exhibit the set of two relaxation peaks: one at intermediate temperature (RT to 250 °C) denoted as R_1, and second one is at high frequency and high temperature region denoted as R_{II}. The activation energy was extracted from log (f) vs. 1/T graphs as shown in Fig. 8a–d for the corresponding relaxation phenomena. The calculated activation energy is equal to 0.24–0.45 eV for parent compound of all measured temperature and frequency intervals. The noted activation energy is in the range of $0.34 \le E_a \le 0.64$ eV, which corresponds to the hopping conduction through single ionized oxygen vacancies ($V_o^{\bullet\bullet}$). This plays a key role

in dielectric relaxation mechanism for all measured samples [19, 34]. Meanwhile, for doped ceramics, two sets of relaxation activation energies were calculated within R_1 and R_2 regions. For R_1 region (low temperature and high frequency region), the calculated activation energies are 0.24–0.65 eV for $x = 0.10$, 0.20 and 0.30 concentrations, respectively. The obtained activation energies at R_1 regions, indicate the relaxations due to thermal motion of localized hopping process of electrons in variable oxidation states of Bi^{3+} ions and single ionized electrons for doped-Aurivillius phase [32, 35]. For R_2 regions, (i.e., at high temperature region) the calculated activation energies are 0.34–0.62 eV, for $x = 0.10$, 0.20 and 0.30 concentrations, respectively as drawn in Fig. 9a–d. However, for doped samples, the oxygen vacancies are formed at high temperature region likely to undoped one. Furthermore, the noted values of activation energy in doped Gd-BBTO ceramics are consistent with the activation energy values in analogous to previous reported materials [32, 35].

7 AC conductivity studies

In general, the ac conductivity originates from the ionic hopping between neighboring potential barriers. The study of ac conductivity based on temperature and/or frequency dependency provides an insight into different relaxation

Fig. 8 a–d The imaginary part of modulus spectroscopy with the variation of frequency at fixed temperatures of the Gd-substituted BaBi$_{4-x}$Gd$_x$Ti$_4$O$_{15}$ ceramics from $x = 0.00$ to 0.30, respectively
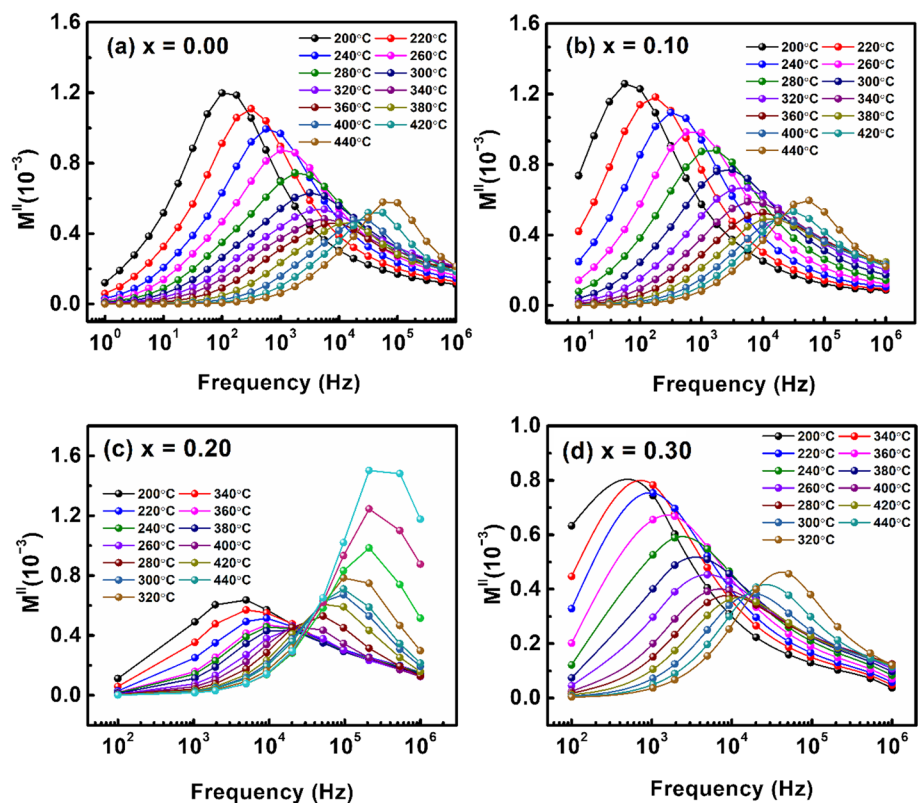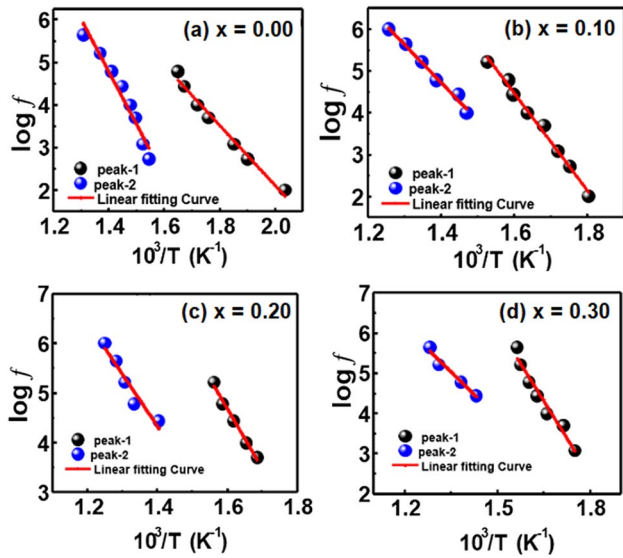
Fig. 9 a–d Calculation of activation energy from Imaginary part of impedance plots by using Arrhenius's plots: log f vs. $10^3/T$ of Gd-doped $BaBi_{4-x}Gd_xTi_4O_{15}$ ceramics $(0.0 \leq x \leq 0.30)$

mechanisms. The ac conductivity of ceramic samples of thickness t and cross-sectional area (A) may be calculated using the real (Z') and imaginary parts ($Z\varepsilon$) of impedance as follows:

$$\sigma_{ac} = \frac{t}{A} \frac{(Z')^2}{(Z')^2 + (Z\varepsilon)^2}. \tag{8}$$

8 Temperature dependent ac conductivity

The contribution of bound and free charges expresses using the dielectric permittivity (ε_r) and dielectric loss tangent (tanδ) from frequencies (0.5 kHz to 1 MHz) with temperature as illustrated in Fig. 10a–d is by an empirical relation:

$$\sigma_{ac} = 2\pi f \varepsilon_0 \varepsilon_r \tan\delta. \tag{9}$$

With increasing temperature, the conductivity of the ceramics is increasing gradually until it reaches a temperature 300 °C, after which an abrupt increase with a significant change of slope is noticed. The sharp variation in slope observed at a specific temperature can often be attributed to a statically disordered lattice, as previously noted [36]. Moreover, there is a discernible hump near the 415 °C, which corresponds to the phase transition temperature in dielectric permittivity vs temperature plot. Sorokin et. al, reported that a jump of conductivity by some definite factor with temperature indicates a phase transition resulting from a change in structural symmetry [37]. A clear hump is detected, especially at low frequencies, for all the Gd

Fig. 10 a–d The plots of ac-conductivity curves with variation of temperature for Gd-doped $BaBi_{4-x}Gd_xTi_4O_{15}$ ceramics from $x=0.00$ to 0.30, respectively
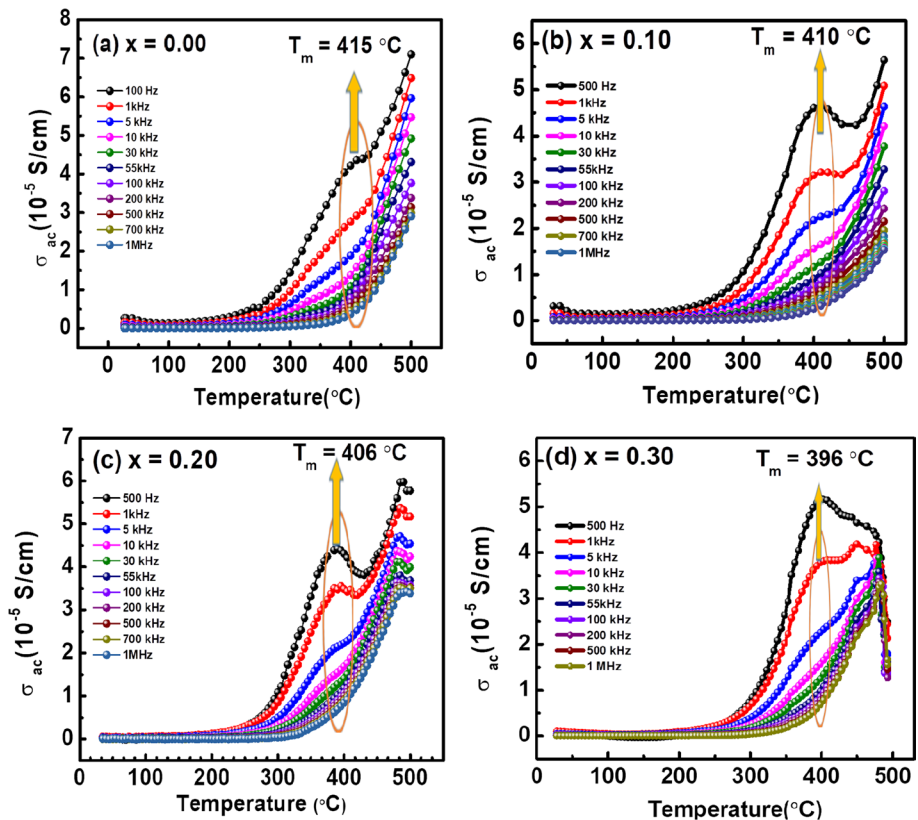
substituted BBTO ceramics. These humps correlate to the ferroelectric to paraelectric phase transition temperature (Tm) obtained in ε_r vs T graph. For the pristine ceramic $x = 0.00$, the hump was noted at 415 °C, and for Gd^{3+} substituted BBTO ceramics with x values of 0.10, 0.20 and 0.30, the Curie temperature (T_m) appear at 410 °C, 406 °C, and 396 °C, respectively. This indicates that the paraelectric to ferroelectric phase transitions in Gd doped ceramics shift towards room temperature [19, 23].

Furthermore, as higher is the frequency higher in conductivity is noticed for all measured samples shown in Table-1 with different fixed temperatures (RT 100 °C, and 300 °C). The Curie temperature (T_m) of layered Aurivillius materials is always interlinked with lattice distortion where the pseudo-perovskite interior is inversely related to tolerance factor (t). The decreasing of T_m towards the lower temperature region with the increase of Gd^{3+} substituent in BBTO ceramics is always depends are two main reasons: (i) On the nature (electronegativity) of substituent compound and, (ii) The difference in ionic radii dopant and parent compound well advance with amount of substituent also play a key role leading to structural distortion. The substituent Gd^{3+} (0.94 Å) ionic radii is less than A-site ionic radii's of Bi^{3+} (1.17 Å), therefore average tolerance factor is decreases, hence structural distortion increases. The structural distortion leads to a decrease in orthorhombicity indicating crystal structure symmetry increases continuously [19, 21]. Hence, a decrease in the ferroelectric transition temperature (T_m) in Gd^{3+} ion-doped BBTO ceramics was noticed. Figure 10a–d depicts the temperature dependent ac conductivity measured at several frequencies for Gd-doped BBTO ceramics from $x = 0.00$ to 0.30, respectively. In perovskite systems, charge transport occurs through multiple hopping processes across the potential barrier of the lattice structure or the local environment of other ions/atoms. In general, the ac conductivity was calculated with associated conduction mechanism at a specific frequency of 10 kHz using the formula as mentioned in Eq. 9. The observed ac conductivity (σ_{ac}) values for Gd doped BBTO (concentrations $x = 0.00$–0.30) ceramics at RT, 300 °C, and at the Curie temperature (T_m) were tabulated in Table 1. The observed ac conductivity values indicate

the presence of semiconducting nature for Gd doped BBTO ceramics [38, 39]. The thermally activated relaxation process can be explained based on the Arrhenius law:

$$\sigma = \sigma_0 \exp\left(\frac{-E_a}{k_B T}\right), \tag{10}$$

where σ_0 bears the pre-exponential factor, which is the characteristics of the material, E_a the activation energy (in eV) means the energy required to enable the AC conduction mechanism in the ceramics, k_B Boltzmann constant, and T absolute temperature, respectively. The activation energy can be calculated from the slope of the linearly fitted plot of $\log(\sigma_{ac})$ vs. $10^3/T$, as illustrated in Fig. 11a–d, at three fixed frequencies: 10 kHz, 50 kHz, and 100 kHz, respectively. It is evident that at temperature below 250 °C, the obtained activation energy in the order of 0.23–0.36 eV for all measured samples. For the temperature range of 300–400 °C, the obtained activation energies are in order of 0.5–1.0 eV, which is well above the Curie temperature. Thus, an opposite nature of semiconductor, known as "positive thermal coefficient", was noticed for all Gd-doped BBTO ceramics. In general, the dielectric relaxation mechanism above RT is often related to the oxygen vacancies, particularly at low frequencies the hopping motion of singly or doubly ionized oxygen vacancies can cause the dielectric relaxation mechanism. During sintering process, vacancies are created for volatile atoms like bismuth, and the oxygen vacancies are created to maintain charge neutrality [27, 39]. The conduction electrons are generated from the ionization of oxygen vacancies in perovskite structured oxides, which can be represented in Eqs. (5) and (6).

The conduction electrons (e') form because of the ionization of oxygen vacancies. As per the previous reports, the activation energy ranges between 0.25 and 0.5 eV for $V_o^{\bullet}$ and around 1 eV for $V_o^{\bullet\bullet}$. The plot of $\log(\sigma_{ac})$ vs. $10^3/T$ results in a linear nature, the slope of these straight line enables us to calculate the activation energies, as represented in Fig. 9a–d. The observed activation energies for Gd doped BBTO ceramics correspond to single ionized oxygen vacancies [29].

## 9 Frequency dependence of AC conductivity

The dependence of ac conductivity (σ_{ac}) on the frequency at various temperature intervals can be understood by using the jump relaxation model proposed by Funke [40]. The dependence of AC conductivity on the frequency for the applied field can be explained by double power law, as given by [41]:

$$\sigma_{ac}(\omega) = \sigma_{dc}(0) + A\omega^{n_1} + B\omega^{n_2}, \tag{11}$$

Table 1 Temperature dependent ac conductivity of pure and Gd-doped BBTO Aurivillius ceramics

Dopant concentration x (mol%)	ac conductivity (σ_{ac}) in S/cm at a temperature of		
	30 °C	300 °C	T_m in °C
$x = 0.00$	0.165×10^{-5}	0.28×10^{-5}	4.38×10^{-5}
$x = 0.10$	0.85×10^{-5}	1.96×10^{-5}	4.46×10^{-5}
$x = 0.20$	0.36×10^{-5}	0.36×10^{-5}	4.41×10^{-5}
$x = 0.30$	0.035×10^{-5}	0.64×10^{-5}	5.16×10^{-5}

Fig. 11 a–d Variation of ac-conductivity (σ_{ac}) vs. temperature at fixed frequency ranges the Gd-substituted BaBi$_{4-x}$Gd$_x$Ti$_4$O$_{15}$ ceramics from $x = 0.00$ to 0.30 respectively
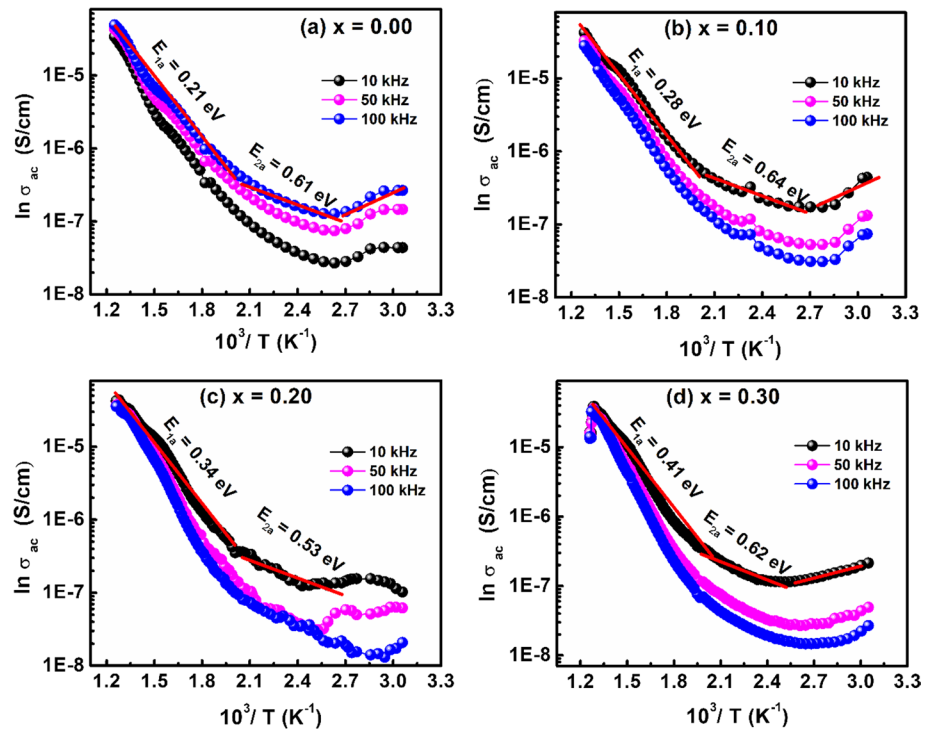
where A, B, n_1 and n_2 are the constants dependent on the temperature and material properties. The term dc conductivity ($\sigma_{dc}(0)$) represents its contribution arising from long-range translational hopping in the long-time limit. The term $A\omega^{n_1}$ indicates the presence of dispersion at low frequencies caused by short range translational (polaron) hopping mechanism, with the exponent value n_1 lying between 0 and 1. Meanwhile, the term $B\omega^{n_2}$ indicates the dispersion at high frequencies due to localized or reorientational hopping motion, with the exponent value n_2 lying between 0 and 2. The values of n_1 and n_2 can be obtained as functions of temperature obtained from the fitted data for the Gd doped BBTO ceramics as displayed in Table 2. Figure 12a–d shows the ac conductivity vs. frequency for the Gd doped BBTO ceramics from concentration $x = 0.00$–0.30 mol% within the temperature range of 40–480 °C. Particularly at

high temperature regimes, the ac conductivity shows a frequency independent nature (plateau) at lower frequencies, indicating the contribution from the dc conductivity [26, 34, 42]. Meanwhile, an appreciable dispersion mechanism was noticed at higher frequencies, commonly attributed from the dispersion, and hopping rate of charge carriers. The hopping motion of charge carriers is typically consistent with the existence of a high density of states in the materials with a band gap resembling that of a semiconductor. The localization of charge carriers results in formation of polarons and the conduction mechanism due to hopping between the nearest neighboring sites. This conductivity mechanism can be explained based on the jump relaxation model or correlated barrier hoping mechanism (CBM) [43].

Table 2 The temperature dependent exponent (n_2) and dc conductivity $\sigma_{dc}(0)$ values of pure and Gd-doped-BBTO ($x = 0.00, 0.10, 0.20,$ and 0.30) Aurivillius ceramics

Temperature (°C)	σ_{dc} ($x = 0.00$)	σ_{dc} ($x = 0.10$)	σ_{dc} ($x = 0.20$)	σ_{dc} ($x = 0.30$)
250	1.24×10^{-8}	1.65×10^{-8}	6.53×10^{-8}	6.06×10^{-8}
280	1.35×10^{-8}	5.30×10^{-7}	3.50×10^{-7}	3.73×10^{-7}
320	2.22×10^{-7}	3.60×10^{-7}	8.16×10^{-7}	2.27×10^{-6}
350	2.25×10^{-6}	2.10×10^{-6}	2.17×10^{-6}	3.63×10^{-6}
380	3.13×10^{-6}	2.56×10^{-6}	2.80×10^{-6}	4.10×10^{-6}
420	3.65×10^{-6}	2.83×10^{-6}	3.18×10^{-6}	4.20×10^{-6}
450	4.00×10^{-6}	2.87×10^{-6}	5.90×10^{-6}	7.16×10^{-6}
	$0.80 \leq n_2 \leq 0.75$	$0.82 \leq n_2 \leq 0.94$	$0.84 \leq n_2 \leq 0.95$	$0.86 \leq n_2 \leq 0.98$

Fig. 12 Jonscher's Power law fitting curves between ac-conductivity (σ_{ac}) vs. frequency for the Gd-substituted BaBi$_{4-x}$Gd$_x$Ti$_4$O$_{15}$ ceramics from $x = 0.00$ to 0.30, respectively
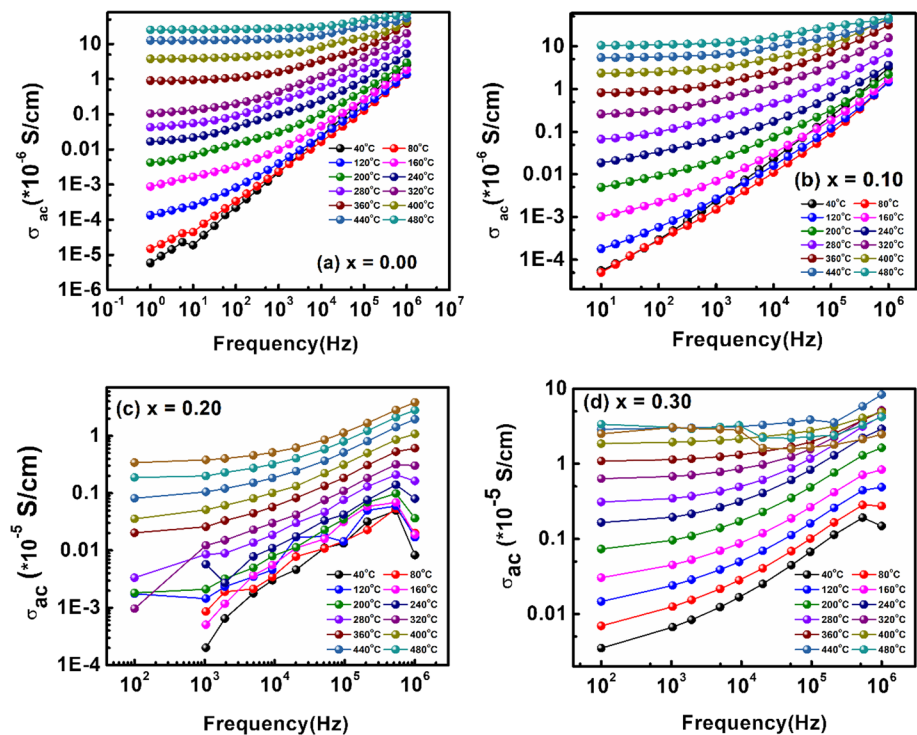
10 Conclusion

In summary, in depth involution of Gd^{3+} ion into BBTO Aurivillius ceramics of orthorhombic crystal system with A2$_1$am space group was explained in detail using X-ray diffraction and room temperature microstructural Raman spectroscopic studies. It is demonstrated using a temperature dependent conductivity study to confirm phase transitions and shifting to low temperature region as noticed with increase of Gd^{3+} ion dopant. A diffuse relaxor activity for low concentration of $x \leq 0.10$ is achieved. Furthermore, $x \geq 0.10$ concentration, the observed classical ferroelectric nature was explained with modified Curie–Weiss law and normalized dielectric permittivity theory. The diminishing of oxygen vacancies with the increase of dopant concentration was demonstrated by frequency and temperature dependent modulus spectroscopic study. The existence of different dielectric relaxations due to the thermal motion of the localized hopping process of electrons in variable oxidation states of different singly ionized ions that depart from ideal Debye behavior was demonstrated using frequency dependent modulus spectroscopic study. Using Jonscher power law, it is demonstrated the different contributions of the electrical behavior in different regimes with given measured temperature intervals. The frequency dependent ac-conductivity study in wide frequency regions from 100 Hz to 1 MHz suggested that the long-range translational hopping in the long-time limit and at low frequency regions. This is caused by short range translational (polaron) hopping

mechanism correlated with jump relaxation model/correlated barrier hoping model. Therefore, the substitution of Gd^{3+} ion in BBTO Aurivillius ceramics plays a vital role to convert a defect free soft ferroelectric material for electronic device applications.

References

1. C.A.-P. de Araujo, J.D. Cuchiaro, L.D. McMillan, M.C. Scott, J.F. Scott, Nature **374**, 627 (1995)
2. J. F. Scott, Berlin (2000).
3. J. Carreaud, P. Gemeiner, J.-M. Kiat, B. Dkhil, C. Bogicevic, T. Rojac, B. Malic, Phys. Rev. B **72**, 174115 (2005)
4. A.A. Bokov, Z.-G. Ye, J. Mater. Sci. **41**, 31 (2006)
5. B. Aurivillius, Ark. Kemi **1**, 463 (1949)
6. E.C. Subbarao, J. Phys. Chem. Solids **23**, 665 (1962)
7. A. Ando, T. Sawada, H. Ogawa, M. Kimura, Y. Sakabe, Jpn. J. Appl. Phys. **41**, 7057 (2002)
8. P. Nayak, K. Mitra, S. Panigrahi, Mater. Lett. **216**, 54 (2018)
9. B.J. Kennedy, Q. Zhou, Y. Kubota, K. Kato, J. Solid State Chem. **181**, 1377 (2008)
10. J. Tellier, P. Boullay, M. Manier, D. Mercurio, J. Solid State Chem. **177**, 1829 (2004)

11. S.K. Rout, E. Sinha, A. Hussian, J.S. Lee, C.W. Ahn, I.W. Kim, S.-I. Woo, J. Appl. Phys. **105**, 24105 (2009)

12. P. Fang, H. Fan, Z. Xi, W. Chen, Solid State Commun.Commun. **152**, 979 (2012)

13. J.D. Bobić, M.M.V. Petrović, N.I. Ilić, E. Palaimiene, R. Grigalaitis, C.O. Paiva-Santos, M. Cilence, B.D. Stojanović, Ceram. Int. **41**, 309 (2015)

14. I. Pribošič, D. Makovec, M. Drofenik, J. Eur. Ceram. Soc. **21**, 1327 (2001)

15. J. Chen, Z. Tang, B. Yang, S. Zhao, Appl. Phys. Lett. **113**, 153904 (2018)

16. F. Rehman, L. Wang, H.-B. Jin, P. Ahmad, Y. Zhao, J.-B. Li, J. Alloys Compd. **709**, 686 (2017)

17. P. Fang, H. Fan, J. Li, L. Chen, F. Liang, J. Alloys Compd. **497**, 416 (2010)

18. J.D. Bobić, M.M.V. Petrović, J. Banys, B.D. Stojanović, Ceram. Int. **39**, 8049 (2013)

19. T. Patri, A. Ghosh, M.L.V. Mahesh, P.D. Babu, S.K. Mandal, M.N. Singh, Sci. Rep. **12**, 16508 (2022)

20. S. Kumar, K.B.R. Varma, J. Phys. D Appl. Phys. **42**, 75405 (2009)

21. T. Patri, T. Durga Rao, K. Chandra Sekhar, S. Raghupathi Rao, S. Rayaprol, P.D. Babu, Phys. Status Solidi **259**, 2200223 (2022)

22. H. Hao, H.X. Liu, M.H. Cao, X.M. Min, S.X. Ouyang, Appl. Phys. A **85**, 69 (2006)

23. P.S. Dobal, R.S. Katiyar, J. Raman Spectrosc.Spectrosc. **33**, 405 (2002)

24. M. Reddyprakash, S.K. Rout, A. Satapathy, T.P. Sinha, S.M. Sariful, Ceram. Int. **42**, 8798 (2016)

25. Y. Chen, J. Xu, S. Xie, Z. Tan, R. Nie, Z. Guan, Q. Wang, J. Zhu, Materials (Basel). **11**, 821 (2018)

26. D.Y. Suárez, I.M. Reaney, W.E. Lee, J. Mater. Res. **16**, 3139 (2001)

27. J.P. Kumar, K.C. Sekhar, T.D. Rao, P.D. Babu, P. Tirupathi, J. Mater. Sci. Mater. Electron. **32**, 9675 (2021)

28. K. Chandra Sekhar, M.L.V. Mahesh, T. Sreenivasu, Y. Rama Krishna, K. Chandra Mouli, P. Tirupathi, J. Mater. Sci. Mater. Electron. **32**, 8628 (2021)

29. T.-F. Zhang, X.-G. Tang, Q.-X. Liu, S.-G. Lu, Y.-P. Jiang, X.-X. Huang, Q.-F. Zhou, AIP Adv. **4**, 107141 (2014)

30. K.C. Sekhar, T. Sreenivasu, K.V. Babu, K. Banerjee, S. Asthana, K.C. Mouli, P. Tirupathi, Ceram. Int. **49**, 8313 (2023)

31. F. Rehman, H.-B. Jin, L. Wang, A. Tanver, D.-Z. Su, J.-B. Li, RSC Adv. **6**, 21254 (2016)

32. C. Ang, Z. Yu, L.E. Cross, Phys. Rev. B **62**, 228 (2000)

33. A. Moure, A. Castro, L. Pardo, Prog. Solid State Chem. **37**, 15 (2009)

34. T. Patri, J. Praveen Kumar, A. Ghosh, P.D. Babu, J. Appl. Phys. **128**, 154102 (2020)

35. A.E. Paladino, J. Am. Ceram. Soc. **48**, 476 (1965)

36. C.B. Azzoni, E.R. Mognaschi, G. Siragusa, J. Phys. C Solid State Phys. **19**, 1443 (1986)

37. N.I. Sorokin, Crystallogr. Reports **62**, 629 (2017)

38. S.A. Long, R.N. Blumenthal, J. Am. Ceram. Soc. **54**, 577 (1971)

39. F. Rehman, J.-B. Li, Y.-K. Dou, J.-S. Zhang, Y.-J. Zhao, M. Rizwan, S. Khalid, H.-B. Jin, J. Alloys Compd. **654**, 315 (2016)

40. K. Funke, R. Hoppe, Solid State Ionics **40**, 200 (1990)

41. A. Pelaiz-Barranco, M.P. Gutierrez-Amador, A. Huanosta, R. Valenzuela, Appl. Phys. Lett. **73**, 2039 (1998)

42. A. Khokhar, M.L.V. Mahesh, A.R. James, P.K. Goyal, K. Sreenivas, J. Alloys Compd. **581**, 150 (2013)

43. H. Hassib, A.A. Razik, Solid State Commun.Commun. **147**, 345 (2008)